Synthesis and characterization of $(Ga,In)_2O_3$ nanowires

Author: Elena López Aymerich.
Advisors: Albert Romano Rodríguez and Guillem Domènech Gil
Facultat de Física, Universitat de Barcelona, Diagonal 645, 08028 Barcelona, Spain.*

Abstract: In this work the growth and characterisation of $(Ga, In)_2O_3$ NWs obtained by a CVD using different mixtures of Ga_2O_3 and In_2O_3 are reported. The NWs have been characterised by SEM, XRD and TEM, proving their cubic crystalline nature similar to In_2O_3 and providing the degree of incorporation of Ga in this lattice. Furthermore, gas nanosensors based on single NWs have been fabricated and measured, proving the sensing properties of the synthesized material.

I. INTRODUCTION

Gas sensors are very important electronic devices that have been developed in the last 4 decades due to their need in environmental and industrial air control. Nowadays, a wide variety of sensing devices can be found in the market, but their properties are, in general, not good enough and large research efforts towards their improvement are still being invested. Out of the different devices available, resistive solid state gas sensors are important due to their response to large number of gases, but present several drawbacks, like their poor selectivity and the need to be heated to properly operate and the consequent power consumption. Their sensing principles are based on the variation of the resistance of a semiconductor material in the presence of certain gases [1]. The most used materials to fabricate these devices are metal oxide (MOX) semiconductors and the most accepted sensing mechanism is based on interaction of the surface O-atoms with the gas molecules, with the consequent charge transfer from or to the semiconductor, resulting in a change in resistance.

Currently, one of the gas sensor development lines goes towards the miniaturization of the MOX devices. This is achieved by reducing the material dimensions, with a consequent increase of the surface-to-volume ratio, which results in a higher sensor response and a decrease of the power consumption. In these situations, MOX nanowires (NW) as sensing part of the device are being used [2].

Among the different MOX materials, Ga_2O_3 [3] and In_2O_3 [4] have been proven as efficient gas sensing materials and can be grown in nanowire form [1]. The alloy of these two MOX, however, has been scarcely studied and there is no report on the gas sensing behaviour of this material.

This present work is focused on the growth of $(Ga,In)_2O_3$ nanowires using chemical vapour deposition (CVD), their structural characterization and their initial test as gas sensor.

II. EXPERIMENTAL

A. Chemical Vapour Deposition Growth

One of the CVD techniques used in NWs synthesis is the so-called Vapour-Liquid-Solid (VLS) growth. This method consists in the evaporation of a precursor of the NW material and its transport in gas phase to an area where liquid catalyst particles are present. The precursor is incorporated into the catalyst, forming a eutectic alloy, and when supersaturation of the precursor in the alloy occurs, precipitation takes place at the liquid-solid interface, giving rise to the NW. This is briefly summarised in Fig. 1.

In our case, the precursor material is a mixture of Ga_2O_3 and In_2O_3 nanopowders, with graphite. A constant flux of carrier gas transports the vapour through the chamber where there are the Au (catalyst) sputter-covered Si/SiO_2 samples. Because of the high temperature, the gold is found in small liquid droplets.

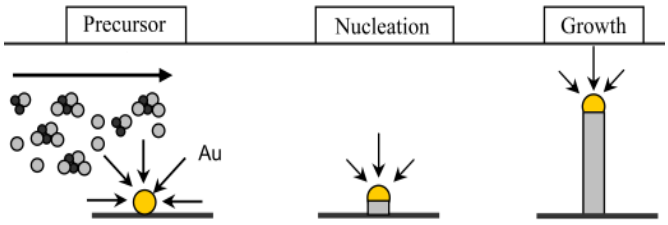

FIG. 1: Sketch of a VLS growing process [5]

The growth process occurs in two ways: in the first the NWs grow in length and is faster, while in the second the NWs grow in axial direction and is slower [6]. This method allows to grow NWs with diameter control ($Ø \leq 100$ nm).

The VLS growth has been carried out in a tubular quartz tube of 5 cm in diameter. The samples used were Si/SiO_2 pieces of 5x5 mm^2, on top of which a thin non-continuous Au layer was sputter-deposited for 5 or 20 s.

Samples were uniformly placed on top of four inverted alumina boats, 0.3 g of the precursor material was placed in an alumina boat. The exact layout is shown in Fig. 2, in which the carrier gas flows downstream, from the left side.

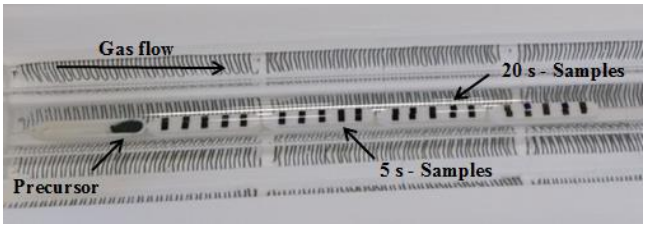

FIG. 2: Image of the final precursor and samples distribution in the furnace.

* Electronic address: elopezay7@alumnes.ub.edu

Different mass ratios of Ga_2O_3 : In_2O_3 : C precursors have been used in this study to cover different Ga- to-In compositions: 2:1:6, 10:1:20 and 1:6:12. These proportions are calculated considering the molecular weight of each precursor and keeping the metal-oxide-to-carbon ratio constant. Graphite is used in this experiment to lower the evaporation temperature of the metal oxide precursor through the carbothermal reaction, in which carbon is oxidized from the metal oxide through reducing the latter, which lowers the evaporation temperature of the process.

A 100sccm (Standard Cubic Centimetres) Ar or Ar/O_2 gas mixture entering from the left of Fig. 2 carries the precursor along the tube, which is kept at atmospheric pressure.

The experiments have been carried out changing the O_2 proportion in Ar flow between 0 and 10 % and the duration of the growth, between 1 and 2 h. The furnace temperature is also controlled at different zones, with the precursor boat maintained at 950 ºC and the substrates, between 850 and 950 ºC.

B. Characterization

All the fabricated samples have been analysed by a Jeol 7100 Field Emission Scanning Electron Microscope (SEM) operating at 15 kV. This type of analysis has allowed us to study the morphology of the samples corresponding to the different employed growing conditions.

Some samples have been further characterized by X-Ray Diffraction (XRD) and Transmission Electron Microscopy (TEM) analysis.

XRD 2θ analysis has been done by a PANalytical X'Pert PRO MRD diffractometer operating with a 0.1541-nm wavelength radiation. To maximize the diffraction signal of the grown material, grazing incidence (GIXRD) configuration is used, with the X-ray beam incident at an angle of 0.5 º to the surface.

The theoretical Bragg's law has been used to estimate the lattice parameter of the NWs according to

$$2\mathrm{d}\sin\theta = n\lambda \qquad (1)$$

where d is the lattice, θ is the angle position of the diffraction peak, n is the peak order and λ is the incident wavelength.

Finally, the TEM analysis has been done with a Jeol J2100 electron transmission microscope, operated at 200 kV to analyse the 2:1:6 sample.

C. Gas measurements

In order to perform the gas sensor measurements, the grown material has been removed from the substrate using sonication in cyclohexane (C_6H_{14}) and some droplets of the solution have been deposited on a microhotplate (MHP). The MHP is a suspended platform that contains interdigitated electrodes and a buried heater. The deposited NWs have been contacted by platinum deposition using a Focused Ion Beam (FIB) system [7].

To make the sensor measurements, the MHP has been mounted on a TO8 support holder and wire bonding has been performed.

The sensor measurements have been done varying the electrical current through the contacted NW and through the heater, independently. The heater current allows to control the MHP temperature between room temperature and 200 ºC. On the other hand, the NW current has been limited to 5 nA to avoid over-heating and damaging the NW.

The gas sensing measurements have been performed inside a self-constructed stainless steel gas chamber, of 8.6 ml volume, connected to a gas mixer with 4 Bronkhorst MassFlow Controllers. A constant gas flow of 200 ml/min was kept for the gas measurements like ethanol, CO and NO_2 diluted in synthetic air (SA, 79 % N_2 and 21 % O_2). Several gas concentrations up to 100 ppm have been used. Two Keithley 2400A Source Measurement Unit allowed controlling the sensor's resistance and MHP heating voltage. The system has been controlled by an home-developed LabVIEW software.

III. RESULTS AND DISCUSSION

A. Scanning Electron Microscopy (SEM)

Fig. 3 shows SEM images of three representative samples corresponding to the three compositions studied and grown under different oxygen concentrations. In all three samples the presence of NWs with lengths between 1 to 3 µm and diameters below 100 nm can be observed. The presence of the Au droplet at the tip of the NWs confirms that they are formed according to the VLS process. In the figures one can also see that the NWs are not straight but show a zig-zag shape. This is a result of a too high growth temperature.

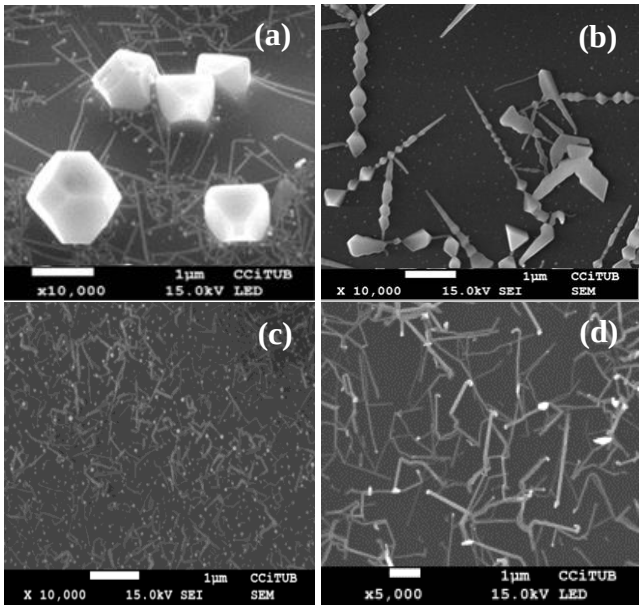

FIG. 3: SEM images of the selected samples growed at 950 ºC in the first and the second furnace zones and: (a) and (b) 2:1:6 sample containing NWs, octahedral and nanorod structures (0.1 % O_2), (c) 1:6:12 sample where only NW can be seen (0 % O_2), (d) 10:1:20 sample (10 % O_2), again, showing only NWs.

In several samples, a coexistence of NWs and other structures can be noticed, as Fig. 3a and b show, such as nanorods (NR) and octahedral structures. The latters, can be interpreted as growing according to a Vapour-Solid (VS) mechanism, motivated by an In-excess in the vapour phase of the precursor. On the other hand, NR can be considered a mixture of VLS NWs and VS octahedral growths [8].

B. X-Ray Diffraction (XRD)

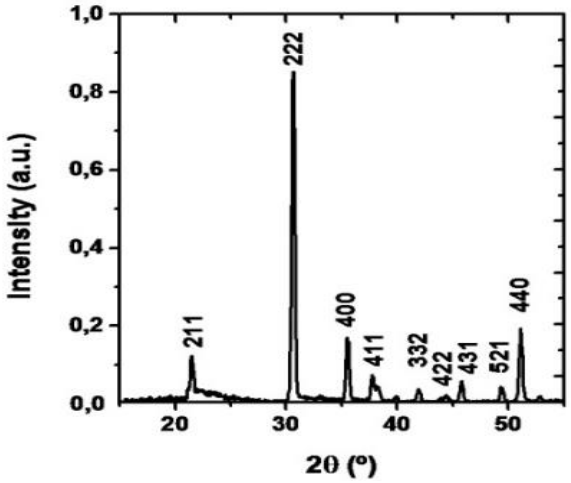

FIG. 4: Measured XRD diagram of $(Ga,In)_2O_3$ 2:1:6 sample. The peaks are identified assuming a cubic phase close to the In_2O_3.

Fig. 4 shows the XRD diagram obtained for sample 2:1:6. The peaks that appear are very close to those reported for In_2O_3 and suggest that the synthesised material crystallise in the cubic structure. Similar patterns have been obtained for the different measured samples. However, in all of them, a displacement and an increase of the Full Width at Half Maximum (FHWM) of the diffraction peaks is observed in comparison with the In_2O_3 samples, as shown in Fig. 5 for the (2 2 2) diffraction peak. These measurements are reported in table I.

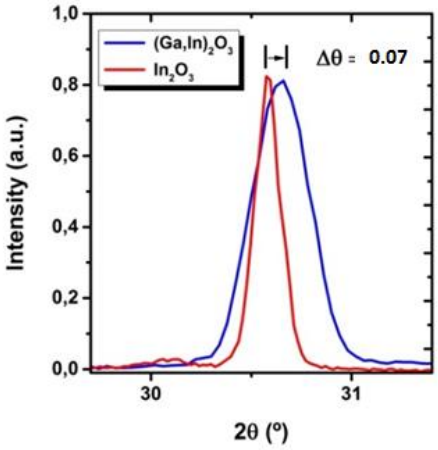

FIG. 5: Comparison of the (2 2 2) diffraction peak from $(Ga,In)_2O_3$ 2:1:6 sample and from the In_2O_3 reference material.

Using Bragg's law (1), we can deduce that a shift of the peak towards higher angles is a consequence of the diminution of the lattice parameter (d), for which the Miller coefficients for the peak evaluated are $h = k = l = 2$, the peak order will be $n = \sqrt{h^2 + k^2 + l^2} = \sqrt{12}$ and, thus, the lattice parameter can be estimated.

Sample	2θ (º)	Δθ (º)	d (Å)	% Ga	FWHM (º)	L (nm)
2:1:6	30.65	0.07	10.097	1.06	0.33	25
10:1:20	30.63	0.05	10.103	0.74	0.34	24
1:6:12	30.59	0.01	10.117	0.02	0.16	51

TABLE I: Position and width of the (2 2 2) peaks for different samples, as well as obtained Ga incorporation and estimated crystalline domain.

These lattice parameter variations can be interpreted as the consequence of the introduction of an external atom in the cubic structure of In_2O_3. In this case, this would be the substitution of the In-atom by Ga-atom. This type of situations can be represented by the Vegard's law [9], that allows quantifying the average substitutional Ga, which can be described as:

$$a_{(Ga,In)_2O_3} = a_{Ga_2O_3}(1 - X) + a_{In_2O_3}X \qquad (2)$$

where X is the amount of Ga in the lattice. Using the reported indium ($a_{In_2O_3} = 10.117$Å) and gallium oxide ($a_{Ga_2O_3} = 8.238$Å) cubic lattice parameters the amount of Ga deduced is reported in table I.

The results show that the percentages of Ga introduced vary from 0 to 1.06 %. These values are much lower than the atomic concentration in the precursor mixture composition.

This behaviour is in agreement with the difference in formation enthalpy for both oxides (ΔH^o_{In2O3}=-222.47 kcal/mol, ΔH^o_{In2O3}=-259.90 kcal/mol). The lower value for In_2O_3 indicates that the probability that the carbothermal reduction of In_2O_3 occurs is higher and, thus, the amount of In_2O_3 precursor in the gas phase is much higher than that of Ga_2O_3, even with a much larger Ga_2O_3 molecular concentration in the precursor phase for the 1:6:12 mixture.

FWHM is also shown in table I. This peak parameter can be interpreted by the Scherrer's equation (3) as inversely proportional to the crystalline dimensions [10].

$$L = \frac{K\lambda}{\beta \cos\theta} \qquad (3)$$

where L is the crystallite domain, K is a constant related to crystallite shape normally taken as 0.9, λ is the XRD wavelength, β is the FWHM and θ is the angle of the diffraction peak. The L value is reported in table I.

The results suggest that the larger FWHM value from the higher Ga-containing samples is either due to smaller NWs or smaller crystalline domains. Because SEM images of Fig. 3 show the opposite results, the smaller domains seem the correct interpretation. To confirm this, more samples analysis is required.

Furthermore, this variation of the crystallite domain can be motivated due to structural defects in NWs lattice, which involve a decrease of the L value. Therefore, according to the results shown in table I, samples 10:1:20 and 2:1:6 should have a higher presence of these defects rather than sample 1:6:12.

C. Transmission Electron Microscopy (TEM)

The analysis realized with TEM has confirmed the previous results obtained by XRD. The images shown in Fig. 6 have been taken both in image and diffraction mode.

In Fig. 6 a, the structure of one single NW of the 2:1:6 samples can be seen. It is clear that the diameter of the NW has changed during the growth, being wider at its base. This could be due to a change in temperature during the growth process. Additionally, the presence of Au at the tip of the NW confirms the VLS catalyst assisted growth of the NWs.

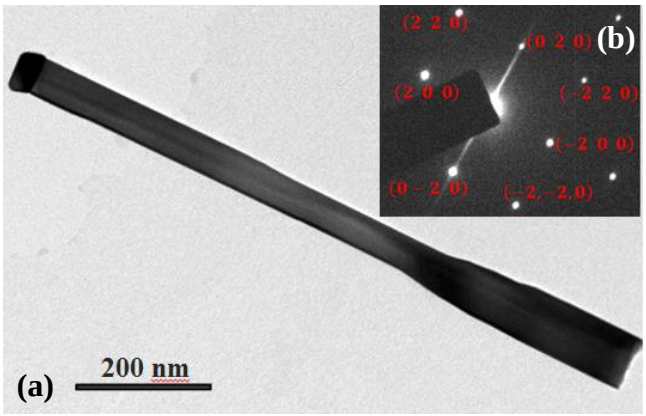

FIG. 6: TEM images of the (a) NW of the samples 2:1:6 and the (b) corresponding electron diffraction image.

Fig. 6 b shows the corresponding diffraction pattern, which is characterized by a regular diffraction spots distribution that prove that the NW is monocrystalline. Moreover, because XRD has proven the cubic phase of the material, the indexation of the pattern has been carried out assuming this phase and has allowed to clearly identify the crystallographic planes. Furthermore, comparing image and diffraction patterns, the determination of the growth direction of this NW can be carried out and is [100]. To determine, whether this, the preferential growth direction in this sample, further need to be analyse and this is the beyond the scope of this work.

IV. GAS SENSING BEHAVIOUR

Prior to the gas sensing measurements, the calibration resistance-temperature curve has been measured for one of the bonded NWs, varying the heater temperature and maintaining the 5nA current flowing through the NW, as shown in Fig. 7.

It is noticeable that the sensor's resistance decreases while the temperature increases, confirming the semiconducting behaviour of the NW. Furthermore, during the gas sensor operation, modification of the resistance will occur when the gas is introduced into the measuring chamber.

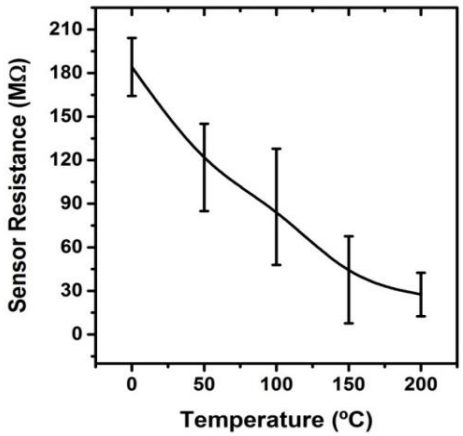

FIG. 7: Sensor resistance of a single NW from samples 2:1:6 as a function of the heater temperature and measuring current 5 nA.

Because both In_2O_3 and Ga_2O_3 are generally n-type semiconductors, it is expected that the synthesised $(Ga,In)_2O_3$ will also be of the same character. Accordingly, the interaction of the material with a reducing gas, like CO, gives rise to a NW's resistance decrease, while the opposite behaviour is expected for an oxidizing one, like NO_2. The sensing mechanisms for these types of gases are represented in Fig. 8.

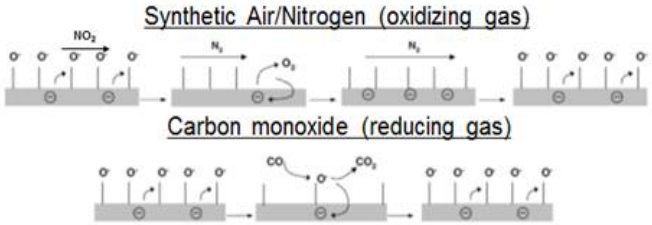

FIG. 8: Sketches of the interaction of the gas sensor surface and an oxidizing and a reducing gas.

In this work we have measured the response of the sensors towards ethanol gas diluted in dry SA. 1h gas pulses have been employed to study both the adsorption and desorption of the gas and this is shown in Fig. 9 at a temperature of 200 ºC for sample 2:1:6, which has been observed to provide the highest gas response. The observed result, reduction of the resistance of the sensor, is in agreement with the reported reactor character of ethanol reported for other MOX sensors.

Furthermore, it is clear that the resistance variation is larger with increasing ethanol in the mixture, confirming the sensing behaviour.

Depending on the gas concentration the sensor response goes from 35 to 80 %, and the response time, defined as the time from 10 to 90 % of the steady state resistance variation, goes from 40 to 800 s. As the response time at 150 ºC goes from 500 to 1150 s, the optimal operation temperature of this sensor is 200 ºC. The recovery signal, however, is much slowly, indicating that the gas desorption process is the limiting under these conditions.

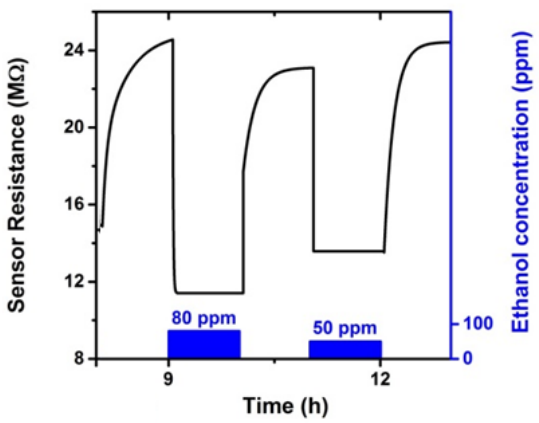

FIG. 9: Sensor Resistance variation in front of ethanol diluted in SA with the microhotplate operating at 200 ºC.

The response obtained for In_2O_3 [4] NWs under these conditions was found below a 30 % indicating that the here fabricated $(Ga,In)_2O_3$ NW based gas sensor gives a higher signal.

V. CONCLUSIONS

In this work, the growth of $(Ga, In)_2O_3$ NWs using the VLS mechanism has been carried out. Different mass ratios of Ga_2O_3 - In_2O_3 - C precursors have been used in order to obtain different stoichiometries in the NW's structure. Due to the different formation enthalpy of the precursors, the incorporation of Ga in the lattice is very low, being about 1 % for Ga_2O_3-rich precursor. While changing the growth conditions, additional nanostructures, like nanorods and octahedral, grew up as the result of the coexistence of VLS and VS growth mechanisms.

XRD analysis proves that the optimal samples have cubic lattice and there is a small deviation of the lattice parameter compared to that of cubic In_2O_3. For one specific NW the growth direction has been determined as being [100].

Gas nanosensor based on single $(Ga, In)_2O_3$ NW on top of MHP show that the effective response to ethanol at 200 ºC and that this value is higher than in In_2O_3 single NW based gas sensors.

Finally, I would like to include that this work has allowed me to learn new skills and techniques complementing and improving those acquired during the bachelor degree.

VI. ACKNOWLEDGEMENTS

I would like to sincerely acknowledge Guillem Domènech for teaching me how to develop the $(Ga, In)_2O_3$ NW, for his patience and help through this research months we have shared. I would also like to acknowledge Albert Romano for his faith on me, and also for his enlightening advises and supervision.

Finally, I would like to thank my family, my parents and my sister, my friends and Alejandro Hernández, for their support through these months.

---

[1] J. Huang and Q. Wan, "Gas sensors based on semiconducting metal oxide one-dimensional nanostructures," *Sensors*,vol. 9, pp. 9903–9924, 2009.

[2] N. Barsan et al, "Metal oxide-based gas sensor research : How to ?," *Sensors and Actuators B:Chemical*, vol. 121, pp. 18–35, 2007.

[3] I. Peiró, Synthesis and characterisation of Ga_2O_3 nanowires (Treball de Fi de Grau), Universitat de Barcelona, 2016.

[4] G. Domènech-Gil et al, "Gas sensors based on individual indium oxide nanowire," *Sensors and Actuators B: Chemical*, vol. 238, pp.447-454, 2017.

[5] M. Kumar et al, "Tunable synthesis of indium oxide octahedral, nanowires and tubular nanoarrow structures under oxidizing and reducing ambients," *Nanotechnology*, vol. 20, pp. 235-608, 2009.

[6] R. S. Wagner and W. C. Ellis, "Vapour-liquid-solid mechanism of single crystal growth," *Applied Physics Letters*, vol. 4, pp. 89-91, 1964.

[7] F. Hernández-Ramírez et al, "Fabrication and electrical characterization of circuits based on individual tin oxide nanowires," *Nanotechnology*, vol. 17, pp. 55-77, 2006.

[8] N. Singh et al, "The temperature-controlled growth of In_2O_3 nanowires, nanotowers and ultr-long layered nanorods," *Nanotechnology*, vol.20, pp. 195-605, 2009.

[9] L.Vegard, "Die Konstitution der Mischkristalle un die Raumfüllung der Atome," *Zeitschrift für Physik*, vol. 5, pp. 17-26, 1921.

[10] R. Zsigmondy, Kolloidchemie Ein Lehrbuch, Berlin: Springer-Verlag Berlin Heidelberg, 1912.